Links between microscopic and macroscopic fluid mechanics

WM. G. HOOVER[1]* and C. G. HOOVER[2]

[1] Department of Applied Science, University of California at Davis/Livermore,
Livermore, CA 94551-7808, USA
[2] Methods Development Group, Lawrence Livermore National Laboratory,
Livermore, CA 94551-7808, USA

The microscopic and macroscopic versions of fluid mechanics differ qualitatively. Microscopic particles obey time-reversible ordinary differential equations. The resulting particle trajectories $\{q(t)\}$ may be time-averaged or ensemble-averaged so as to generate field quantities corresponding to macroscopic variables. On the other hand, the macroscopic continuum fields described by fluid mechanics follow irreversible partial differential equations. Smooth particle methods bridge the gap separating these two views of fluids by solving the macroscopic field equations with particle dynamics that resemble molecular dynamics. Recently, nonlinear dynamics have provided some useful tools for understanding the relationship between the microscopic and macroscopic points of view. Chaos and fractals play key roles in this new understanding. Non-equilibrium phase-space averages look very different from their equilibrium counterparts. Away from equilibrium the smooth phase-space distributions are replaced by fractional-dimensional singular distributions that exhibit time irreversibility.

1. Introduction

An understanding of fluid mechanics [1, 2] requires the simultaneous acceptance of two seemingly disparate views, the atomistic microscopic view and the laboratory-scale continuum macroscopic view. To follow Voltaire, we begin here by describing these two versions of fluid mechanics. The microscopic version deals with moving particles while the macroscopic one describes developing fields. This difference is intrinsic. At a minimum, some kind of averaging process, either time averaging or ensemble averaging, over $\{qp\}$ phase space, is required if the two types of mechanics are to correspond.

The two views differ in time symmetry too. The microscopic version is time reversible while the macroscopic one is almost always not, again suggesting intrinsic differences. At equilibrium, Boltzmann and Gibbs successfully formulated the phase-space averages necessary to achieve correspondence between the two mechanics. Such microscopic averages are the basis of 'statistical mechanics'. At equilibrium the phase-space probability densities $f(q, p, t)$ characterized by Boltzmann and Gibbs vary smoothly, as exponentials of appropriate potential functions. Away from equilibrium the phase-space probabilities become distributions, which are singular everywhere, making the averaging problem much harder [1, 3–7]. In the non-equilibrium

case the phase-space trajectories become irreversible despite reversible motion equations!

The problem of understanding the differences in time reversibility was emphasized by Loschmidt and repeatedly attacked by Boltzmann. Computational research efforts over the past 20 years have made a further advance toward understanding non-equilibrium systems by showing that the irreversibility of non-equilibrium flows is linked closely to the concepts of chaos, Lyapunov instability, and fractals.

Progress is slow. We start out here with Euler, Hamilton, Lagrange, and Newton, and we end up with very recent work. We dedicate this review to Dominique Levesque, whose work has influenced our own, both in the early days of molecular dynamics simulations [8] and much more recently [9]. Dominique has helped us in our efforts to understand the connections between time reversibility, computer simulations and chaos [4].

2. Microscopic mechanics

The conventional microscopic mechanism for particle motion is the Hamiltonian function $H(q, p)$, which is the total energy expressed as a function of coordinates and momenta. For simple fluids, described with Cartesian coordinates, the Hamiltonian may be separated into potential and kinetic energies:

$$H(q, p) = \Phi(q) + K(p) = \Phi(q) + \sum \frac{p^2}{2m}.$$

* Author for correspondence. e-mail: redskunk@starband.net

In this simple separable case, microscopic computer simulation can use the Newtonian representation of accelerations from forces given by the potential Φ:

$$\dot{p} = m\dot{v} = m\ddot{r} = F = -\nabla_r\Phi(r).$$

Although textbooks often state that it is difficult to solve these equations, particularly if the force F is nonlinear, that view is obsolete. The simple two-step leapfrog algorithm is effective and easy to program:

$$r(t + \mathrm{d}t) = r(t) + v\left(t + \frac{\mathrm{d}t}{2}\right)\mathrm{d}t;$$

$$v\left(t + \frac{\mathrm{d}t}{2}\right) = v\left(t - \frac{\mathrm{d}t}{2}t\right) + \frac{F(t)}{m}\,\mathrm{d}t.$$

Hamilton's motion equations, in $\{qp\}$ phase space, are useful alternatives to Newtonian mechanics:

$$\dot{q} = +\frac{\partial H}{\partial p}; \quad \dot{p} = -\frac{\partial H}{\partial q}.$$

The generalized coordinates q in Hamilton's equations of motion are especially useful for molecular systems or for systems with certain non-equilibrium constraints.

See figure 1 for a simple 'chaotic' equilibrium application of the equations, the motion of a mass point confined in a 'cell' formed by the combined force fields of four fixed neighbours, the 'correlated cell model' [10]. We call motion such as that exhibited by this model 'chaotic': small perturbations δ in the initial conditions have a tendency to grow exponentially quickly with time:

$$\delta(t)/\delta(0) \simeq e^{\lambda t}.$$

As we shall see, chaos plays a key role in connecting the microscopic and macroscopic descriptions of fluids. For a popular account of chaos and its impact on physics see Ford's review [11].

From the standpoint of understanding, the Hamiltonian version has three advantages over the slightly simpler Newtonian formulation: (i) any convenient set of coordinates q may be used; (ii) quantum mechanics is Hamiltonian based; and (iii) the specific identity satisfied by the differentials of Hamilton's equations of motion,

$$\frac{\partial\dot{q}}{\partial q} + \frac{\partial\dot{p}}{\partial p} = \frac{\partial^2 H}{\partial q\partial p} - \frac{\partial^2 H}{\partial p\partial q} \equiv 0,$$

has a useful and interesting corollary, namely Liouville's theorem: the 'comoving' (meaning following the motion) time-dependent probability density in phase space $f(q,p,t)$ is unchanged provided that the motion evolves according to Hamilton's equations. Hamilton's equations are appropriate for describing either 'isolated' or 'closed' systems, systems lacking external sources or sinks of mass, momentum, and energy. The heat trans-
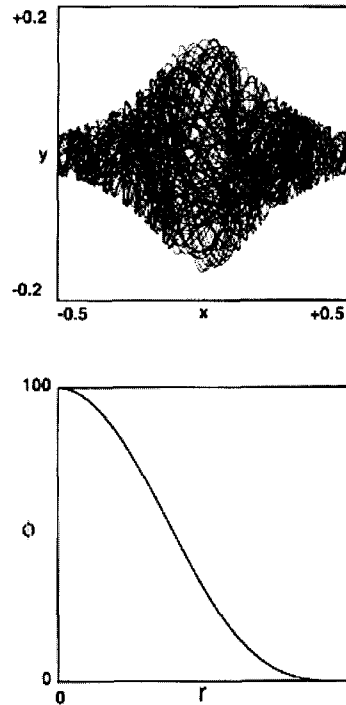

Figure 1. Chaotic trajectory for $0 < t < 100$ for a single particle. The particle is confined to a 'cell' with periodic boundaries [1]. The cell centre is located at the origin. $-\sqrt{1/4} < x < +\sqrt{1/4}$. $-\sqrt{3/4} < y < +\sqrt{3/4}$. The moving particle interacts with four fixed neighbours at $\{\pm\sqrt{1/4}, \pm\sqrt{3/4}\}$ according to the pair potential shown in the figure: $\phi(r) = 100(1 - r^2)^4$. For the total energy $E = (p^2/2m) + \sum_{j=1}^{4}\phi(|r_0 - r_j|) = 1$ the motion is chaotic, and shows Lyapunov instability for small changes in the initial conditions.

fers and/or mass transfers that occur at 'open' systems' boundaries cannot be described by Hamiltonian mechanics.

Liouville's theorem [3, 12] is most readily understood by considering the time-dependent probability of occupying a fixed infinitesimal phase-space volume element $\prod \mathrm{d}q\,\mathrm{d}p$. This many-dimensional volume element has two dimensions for every qp coordinate–momentum pair. The occupancy probability $f(q,p,t)\prod \mathrm{d}q\,\mathrm{d}p$ defines the phase-space probability density at time t, $f(q,p,t)$. The time-rate-of-change of this probability, with the volume element fixed in phase space, is

$$\frac{\partial\left[f(q,p,t)\prod \mathrm{d}q\,\mathrm{d}p\right]}{\partial t} = \prod \mathrm{d}q\,\mathrm{d}p\frac{\partial f}{\partial t},$$

which is given in turn by the summed-up differences between the flows into and out of the element. Provided that f is differentiable, conservation of probability then

provides an exact partial differential equation for the time development of f:

$$\frac{\partial f}{\partial t} \equiv -\sum \frac{\partial(f\dot{q})}{\partial q} - \sum \frac{\partial(f\dot{p})}{\partial p}.$$

As a consequence, $\dot{f}$, the comoving time derivative of $f(q, p, t)$, following the motion, is exactly zero:

$$\frac{df}{dt} \equiv \dot{f} = \frac{\partial f}{\partial t} + \sum \dot{q} \frac{\partial f}{\partial q} + \sum \dot{p} \frac{\partial f}{\partial p}$$

$$= -f \sum \left[\frac{\partial \dot{q}}{\partial q} + \frac{\partial \dot{p}}{\partial p} \right] \equiv 0.$$

This consequence of Hamilton's motion equations, that f following the motion is unchanged, is 'Liouville's theorem'.

Because phase-space volume has a direct physical significance (its logarithm gives the entropy) it is worthwhile to stress an equivalent version of the theorem. Let us describe the evolution of phase volume rather than evolution of density. To do so let us consider an infinitesimal comoving phase-space volume element, abbreviated $\otimes$. Because the total probability within the moving element $\otimes$, $f\otimes$, is necessarily unchanged following the motion, the theorem implies that the comoving volume, Gibbs' 'extension in phase' $\otimes$, is constant also:

$$0 \equiv \frac{d(f\otimes)}{dt} = f\dot{\otimes} + \otimes\dot{f} = f\dot{\otimes} \longrightarrow$$

$$0 = \dot{\otimes} = \frac{d\otimes}{dt} = \frac{\partial\otimes}{\partial t} + \sum \dot{q} \frac{\partial\otimes}{\partial q} + \sum \dot{p} \frac{\partial\otimes}{\partial p}.$$

Liouville's theorem is fundamental to statistical mechanics because it establishes the stationary time-independent form for $f_{eq}(q, p)$. Along any trajectory satisfying Hamilton's equations the 'equilibrium' (stationary) form of f can only be a constant. Liouville's theorem is the 'continuity equation' in phase space. The more familiar continuity equation for the evolution of fluid (or solid) mass density ρ in ordinary space is discussed in the next section.

The coordinate evolution according to Hamilton's equations of motion is time reversible [4, 5]. This exact reversibility even carries over to some specially designed 'bit-reversible' computer algorithms pioneered by Levesque and Verlet [9, 13]. This reversibility means that either of the two time orderings $t = \pm n \, dt$ of a coordinate sequence solving the motion equations

$$\{q_{-n}, q_{-n+1}, \ldots, q_{n-1}, q_n\} \text{ or } \{q_n, q_{n-1}, \ldots, q_{-n+1}, q_{-n}\},$$

is an equally valid solution of the motion equations. The initial and final conditions simply exchange roles in the two solutions.

The basis for this very restrictive property of time reversibility is phenomenological. It lies at the heart of all the fundamental physical laws. And this same reversibility property is particularly useful for analysis [5], as we shall see.

The microscopic mechanical equations also conserve energy, as must any macroscopic equations describing the behaviour of points aggregated together into a continuum. The macroscopic continuum viewpoint is more aptly and simply described by the macroscopic mechanics developed to describe continua. Numerical continuum descriptions have an additional advantage over their microscopic cousins. Continuum simulations can employ a much longer timestep dt (the interval between successive particle- or field-variable evaluations) than do microscopic simulations. The continuum description is governed by the sound traversal time while the microscopic description is governed by the atomic collision time.

3. Macroscopic mechanics

From the macroscopic point of view, motion is controlled by 'constitutive relations' (including thermal and mechanical 'equations of state' as well as phenomenological relations like Fourier's law for heat flow or Newton's corresponding law for viscous flow) that describe the dependence of the temperature, the pressure tensor and the heat flux on density, velocity, energy and their gradients. Provided that the continuum field properties vary smoothly in space and time, these resulting density, velocity and energy fields follow simple partial differential equations.

The time histories of the mass density (or composition), velocity and energy are consequences of conservation of mass, momentum and energy. The governing partial differential equations follow from analyses of the flows of mass, momentum and energy into and out of a fixed 'control volume' $dx\,dy\,dz$, an infinitesimal volume element. By choosing the control volume sufficiently small, the net flows in and out may be expressed in terms of the gradients of the corresponding fluxes. The mass flow is simplest. The mass within the control volume $dx\,dy\,dz$ changes due to the slight differences in the mass fluxes ρv at opposite sides of the volume:

$$x \pm \frac{dx}{2}, \quad y \pm \frac{dy}{2}, \quad z \pm \frac{dz}{2}.$$

During the short time interval dt the mass change due to flow in the x direction is

$$[-(\rho v_x)_{x + dx/2} + (\rho v_x)_{x - dx/2}] \, dy \, dz \, dt$$

$$\simeq -\frac{\partial(\rho v_x)}{\partial x} \, dx \, dy \, dz \, dt.$$

Thus the total density change due to velocity gradients, summed up over all three directions x, y, z, is described by the 'continuity equation'

$$\frac{\partial \rho}{\partial t} = -\nabla \cdot (\rho v),$$

in the fixed Eulerian frame. The equivalent expression, following the motion with the local velocity v, gives the Lagrangian (comoving) form of the continuity equation:

$$\dot{\rho} = \frac{\partial \rho}{\partial t} + v \cdot \nabla \rho = -\rho \nabla \cdot v.$$

The momentum in the control volume $\rho v \, dx \, dy \, dz$ itself responds to gradients in the force per unit area on the faces $dx \, dy$, $dy \, dz$, and $dz \, dx$ as well as to convective flows of momentum into and out of the element. The quotients, forces divided by area (defined in the (Lagrangian) coordinate frame moving with the material, where convective effects are eliminated) define the components of the pressure tensor P. The governing partial differential equation for the acceleration of a small mass in the comoving frame gives the Lagrangian 'equation of motion'

$$\rho \dot{v} = \rho \left(\frac{\partial v}{\partial t} + v \cdot \nabla v \right) = -\nabla \cdot P.$$

The equivalent Eulerian equation of motion, in the fixed 'control-volume' frame includes the convective flow of momentum also:

$$\frac{\partial(\rho v)}{\partial t} = -\nabla \cdot (P + \rho v v).$$

In either case note that changing the signs of the velocity v and the time t leaves both the continuity equation and the equation of motion unchanged, so that they look time reversible.

But appearances can be deceiving. The explicit irreversibility in the equation of motion becomes apparent when, as is often the case, the pressure tensor P depends on velocity gradients, so that the forces going forwards and backwards in time can differ. In a 'Newtonian' fluid the time-irreversible viscous forces are exactly proportional to the components of the velocity gradient tensor ∇v.

Despite this overall irreversibility, the continuum equation of motion continues to conserve energy just as does its microscopic counterpart. But a new pair of variables, associated with heat transfer rather than work, is present in the continuum description of thermodynamics and hydrodynamics. These are temperature and entropy (section 5). Although strictly these thermal variables are defined only at equilibrium, it is tempting if not irresistible, and often even useful, to consider them for non-equilibrium processes too.

In the non-equilibrium case the second law of thermodynamics states that the overall entropy S can only increase as time goes on. Because temperature is a state variable, independent of the direction of time, Fourier's phenomenological law (that heat flows from hot to cold) also violates time reversibility, just as does Newtonian viscosity, which insists that work must be done to maintain a velocity gradient. Any time-reversible microscopic theory claiming to compute an analogue of the macroscopic thermodynamic entropy S must surmount the difficulty of dealing with irreversibility: the second law of thermodynamics, with Fourier's law of heat flow and with Newtonian viscosity. Temperature carries over to non-equilibrium systems better than does entropy. For an introduction see sections 5, 9 and 10 and for a thorough discussion see [4].

4. Smooth particle applied mechanics

The macroscopic fluid equations are most often solved on an initially regular grid of points. The points are either fixed in space (Eulerian) or comoving with the fluid (Lagrangian). Both these approaches can become unstable in sufficiently irregular flows. To avoid such grid-based instabilities, at the price of introducing fluctuations, the grid points' motions may be made to follow individual particle equations of motion, free of instabilities. In this 'particle method' the continuum field variables are represented as smoothly interpolated particle properties. The interpolation is based on a short-ranged weighting function $w(r < h)$. The range h and computational timestep dt govern the convergence and stability properties of this particle method in just the same way as do the space and time increments dx and dt in conventional continuum simulations. Figure 2 shows a typical particle weight function.

The continuum equation of motion, which gives the local fluid accelerations in terms of the pressure tensor gradient there, $\nabla \cdot P$, can then be rewritten as a motion equation for particles, with each particle providing contributions to the continuum fields within a sphere of radius h centred on the particle. The interpolated solutions of the particle equations converge to the solution of the field or continuum equations in the limit that the number of particles increases without bound while the range h approaches zero in such a way that each particle interacts with many neighbouring particles. This particle–field solution method, discovered independently by Lucy and by Monaghan, and since then applied to a wide variety of problems in fluid and solid mechanics, is smooth particle applied mechanics (SPAM) [14–19]. 'Smooth' refers to the differentiability of the associated particle weights and the continuum fields derived from them.
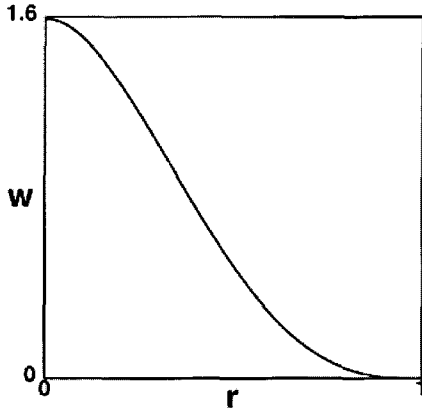
Figure 2. Lucy's weight function, defined in section 4 and used in the free-expansion problem illustrated in figure 3. Note the strong similarity between this weight function and the smooth repulsive pair potential shown in figure 1.

In SPAM, each particle has a fixed mass m. This mass is to be visualized as distributed over space according to the normalized weight function $w(r)$:

$$\int_0^h w_{2D}(r)2\pi r\,dr \equiv 1; \qquad \int_0^h w_{3D}(r)4\pi r^2\,dr \equiv 1.$$

Again see figure 2 for a typical example weight function [15]. The smooth particle mass density $\rho(r)$ at a point r or ρ_i at particle i is given by the contributions of all nearby particles to the summed-up weights:

$$\rho(r) = m\sum_j w(r - r_j); \qquad \rho(r_i) = m\sum_j w(r_i - r_j).$$

More generally the continuum average $C(r)$ of any particle property C_i is given by the definition

$$(C\rho)_r \equiv m\sum_j C_j w(r - r_j) \longleftrightarrow$$

$$C(r) = \sum_j C_j w(r - r_j)/\sum_j w(r - r_j).$$

Notice that the continuum property at r_i, $C(r_i)$, generally is not the same as the particle property there, C_i. Because $w(r)$ is to be chosen with at least two continuous derivatives, both ∇C and $\nabla\nabla C$ are continuous everywhere.

SPAM conserves mass automatically. The integrated density distribution simply reproduces the total system mass. The fluid continuity equation, $\dot\rho/\rho = -\nabla \cdot v$, applied at the location of particle i, gives a useful expression for the velocity divergence:

$$\frac{\dot\rho_i}{\rho_i} \equiv -\nabla \cdot v \equiv \frac{\sum_j v_{ij} \cdot \nabla_i w(r_i - r_j)}{\sum_j w(r_i - r_j)},$$

where v_{ij} is the relative velocity of particles i and j,

$$v_{ij} \equiv v_i - v_j.$$

Gradients $\{\nabla C\}$ of other continuum field variables $\{C(r)\}$ may be obtained by differentiating the definition of $(C\rho)_r$ given above:

$$\nabla(C\rho)_r \equiv \sum_j C_j \nabla_j w(r - r_j).$$

Let us apply this gradient definition to an exact partial differential equation for the motion in a continuum fluid,

$$\dot v \equiv -\frac{1}{\rho}\nabla \cdot P = -\nabla \cdot \frac{P}{\rho} - \frac{P}{\rho^2} \cdot \nabla\rho,$$

choosing the location r in $\nabla(C\rho)_r$ occupied by particle i with velocity v_i. The gradient definitions, with C first equal to $(1/\rho^2)$ and second to 1, then provide the equation of motion for the particle:

$$\dot v_i = -m\sum_j \left[\left(\frac{P}{\rho^2}\right)_i + \left(\frac{P}{\rho^2}\right)_j\right] \cdot \nabla_i w(r_i - r_j)$$

$$\equiv +m\sum_j \left[\left(\frac{P}{\rho^2}\right)_i + \left(\frac{P}{\rho^2}\right)_j\right] \cdot \nabla_j w(r_i - r_j).$$

Note that the gradient of the continuum pressure at the location of particle i is used to accelerate that particle's velocity. The resulting particle equation of motion, although it does not necessarily correspond to central forces, does conserve momentum exactly. The smooth particle equation of motion reduces to ordinary molecular dynamics (with a pair potential proportional to the weighting function $w(r)$) whenever the pressure tensor P and the density ρ vary slowly in space, as is the case not too far from equilibrium. Using SPAM to solve the continuum equations reintroduces the fluctuations (through the relative motions of the particles) that are absent in the more usual grid-based continuum methods.

Figure 3 shows a many-body application of SPAM in two space dimensions, a simulation of the expansion of a compressed gas into a surrounding vacuum [18, 19]. The individual particle locations have been used to compute contours of density and kinetic energy using the simple weight function introduced by Lucy and shown in figure 2:

$$w_{2D}(r) = w_{Lucy}\left(x \equiv \frac{r}{h} < 1\right) = \frac{5}{\pi h^2}(1 - x)^3(1 + 3x).$$
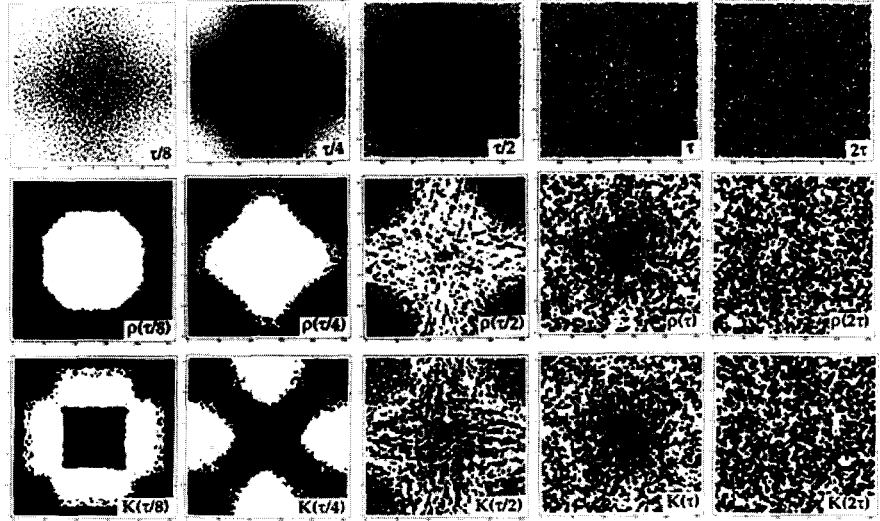
Figure 3. Expansion of 16 384 particles into a surrounding vacuum as treated with SPAM. Snapshots of the particle locations with corresponding density and kinetic energy contours show that the system is essentially uniform after two sound traversal times. Gibbs' microscopic entropy remains constant during the expansion process. See [18, 19] for details of the calculation.

In the free-expansion problem of figure 3 we have used the ideal-gas equation of state appropriate to two space dimensions, $P = \rho e \propto \rho^2$, so that the internal energy per unit mass e is proportional to the mass density ρ. As a consequence, this simple example problem involves solving only the equation of motion. More complicated equations of state require keeping track of internal energy by also solving the 'energy equation',

$$\dot{e} = \frac{-1}{\rho}[\nabla \cdot Q + \nabla v : P],$$

in addition to the equation of motion. The smooth particle version of the energy equation contains both energy changes due to heat flux, associated with the heat-flux vector Q and energy changes due to work done, associated with the pressure tensor P and the velocity gradient tensor ∇v:

$$\dot{e}_i = -m\sum_j\left[\left(\frac{Q}{\rho^2}\right)_i + \left(\frac{Q}{\rho^2}\right)_j\right] \cdot \nabla_i w(r_i - r_j)$$

$$+ \frac{m}{2}\sum_j\left[\left(\frac{P}{\rho^2}\right)_i + \left(\frac{P}{\rho^2}\right)_j\right] : v_{ij}\nabla_i w(r_i - r_j).$$

This energy equation needs to be included in problems like Rayleigh-Bénard flow that involve heat transfer.

5. Temperature and entropy

In thermodynamics temperature and entropy are defined in terms of reversible (near equilibrium) processes involving heat transfer. Temperature is given by the ideal-gas thermometer. It is a measure of the (time or ensemble) averaged kinetic energy of the thermal bath particles making up the ideal-gas thermometer [4, 19, 20]:

$$T \equiv \left\langle\frac{p_x^2}{mk}\right\rangle = \left\langle\frac{p_y^2}{mk}\right\rangle = \left\langle\frac{p_z^2}{mk}\right\rangle.$$

This kinetic energy temperature is defined under the equilibrium condition that the net heat transfer between system and bath vanishes, so that both the system being measured and the measuring bath share the same temperature T. Equilibrium kinetic theory calculations, as introduced by Maxwell and Boltzmann, provide a detailed validation of this thermometer idea. They show that a heavy particle undergoing independent binary collisions with an equilibrium ideal-gas heat bath tends, on a time-averaged basis, towards the mean temperature of the bath [4, 20].

And so long as the states linked by heat transfer are equilibrium states, the integrated heat absorbed in reversible processes linking such states is, when divided by the temperature of heat transfer, the differential of a state function, entropy, $\dot{S} = \dot{Q}_{rev}/T$. The properties of entropy (an extensive state function, additive for independent systems) lead directly to a microscopic equivalent of the entropy,

$$S(N, E, V) = k \ln \Omega(N, E, V),$$

where $\Omega(N, E, V)$ is the number of states available to an N-body fluid system with energy E confined to a volume V. Classically, $\Omega(N, E, V)$ is the available $\{qp\}$ phase volume. Temperature then follows from the energy dependence of entropy. By maximizing the total entropy of a two-part system (by allowing heat transfer between

the two parts) the maximum-entropy state defines the equilibrium temperature:

$$T = \left(\frac{\partial E}{\partial S}\right)_{N,V}.$$

An equilibrium statistical mechanical calculation, based on the energy dependence of the ideal-gas phase-space states, shows that this entropy-based temperature is the same as the kinetic-theory-based ideal-gas-thermometer temperature. The two temperatures are based on kinetic energy and probability density, respectively. For reasons explained in section 9, only the kinetic energy interpretation of temperature is useful far from equilibrium.

6. Averaging, statistical mechanics

The validity of the canonical phase-space distribution, $f(q, p) \propto e^{-H/kT}$, for fluids as well as gases was evidently discovered independently by Gibbs and Boltzmann around 1883 [4]. Both Gibbs [21] and Boltzmann [22] recognized that the complex particle description of microscopic many-body systems could be simplified by averaging, and both men expected that an average over time could be replaced by an average over possible phase-space states. Liouville's theorem, as discussed in section 2, is consistent with this point of view. Liouville's theorem, the equivalent of the continuity equation for the phase-space flow, states that $f(q, p, t)$, the probability density in $\{qp\}$ phase space, flows unchanged according to Hamilton's equations: $\dot{f} \equiv 0$. This means that a constant phase-space density is unchanged by Hamilton's motion equations, and so corresponds to a stationary thermodynamic state for an isolated system with a fixed composition, energy and volume.

Liouville's theorem made it possible to show that the macroscopic thermodynamic entropy $S(N, E, V)$ can be computed by averaging the (logarithm of) the phase-space probability density, $S/k = -\langle \ln f \rangle$. Because the density $f(q, p, t)$ can be nothing more than a superposition of Hamiltonian trajectories, there is a paradoxical logical difficulty in reconciling thermodynamics' inexorable increase of S with the time-reversibility of the underlying Hamiltonian mechanics. One aspect of the paradox may be clarified by studying the details of the free-expansion example of figure 3, the fourfold expansion of a low density ideal gas into a larger volume. Though the microscopic Gibbs' entropy is necessarily unchanged for this expansion, the macroscopic thermodynamic entropy, based on the local energy and density, shows the proper entropy increase. The SPAM calculation of the entropy increase [18, 19] includes the contributions of local velocity fluctuations to the internal energy density of the expanding gas, $\rho(\langle v^2 \rangle - \langle v \rangle^2)/2$. It is these fluctuations (analogous to

heat) that account for the increasing entropy. The smooth particle averaging of these fluctuations can be thought of alternatively as a spatial coarse graining. Evidently fluctuations and averaging are two essential microscopic ingredients of the macroscopic second law of thermodynamics.

The other thermodynamic state-variable properties are straightforward and non-paradoxical, even far from equilibrium. The thermodynamic energy E is just the same as the total energy of the corresponding ensemble of phase-space energy states with energy E:

$$E = \langle \Phi \rangle + \langle K \rangle.$$

Unlike energy, the temperature T and the microscopic pressure tensor P fluctuate. The temperature is computed from the mean value of the kinetic energy while the macroscopic pressure tensor may be related to the time-averaged or ensemble-averaged mechanical boundary forces exerted by the N particles inside the volume V:

$$VP = -\sum \langle rF \rangle + \sum \left\langle \frac{pp}{m} \right\rangle.$$

Thus, the basic thermodynamic equations of state, both thermal and mechanical, $T(N, V, E), P(N, V, E)$ may be
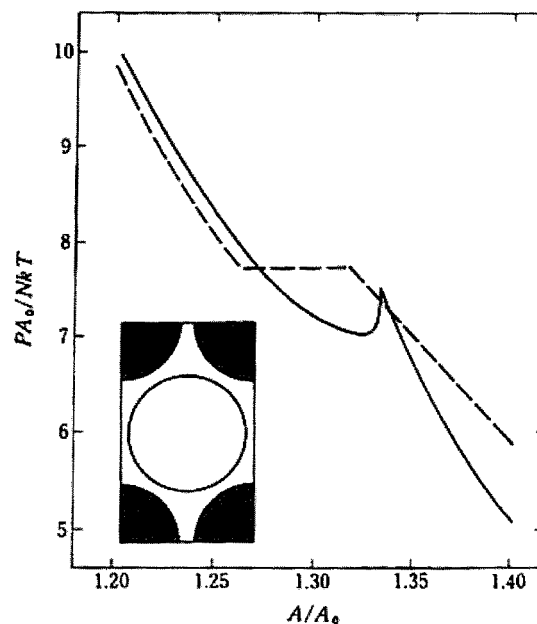

Figure 4. A two-body hard-disc system exhibits a van der Waals loop and realistic diffusion and viscosity coefficients. The loop includes the density (three-fourths the close-packed density) at which the two discs can begin to diffuse. The dashed line indicates the equation of state for large systems of discs. A_0 indicates the close-packed area.

considered as determined by the corresponding microscopic Hamiltonian.

The averages themselves are evaluated by computer simulation 'molecular dynamics'. Temperature is evaluated from the mean kinetic energy, $T \equiv \langle 2K/3Nk \rangle$ in three dimensions and $\langle K/Nk \rangle$ in two, as may be shown by the equilibration with the ideal-gas thermometer of section 5, and pressure is then evaluated from Clausius' 'virial' $\langle \sum rF \rangle$. Around 1970, computer simulations and supporting theoretical work established that realistic equations of state, including phase equilibria like van der Waals' (even with the loop!), could be calculated according to Gibbs' and Boltzmann's prescription.

It is less well known that the number of particles used in the simulations can be relatively small. As an extreme example, the equation of state for a two-particle system of hard discs, with periodic boundaries is shown in figure 4 [10]. It is noteworthy that both the pressure and the density of the phase transition corresponding to the van der Waals' loop are within 10% of values obtained from simulations with thousands of particles [23].

7. Linear response and nonlinear transport

Green [24] and Kubo [25] extended Gibbs' and Boltzmann's equilibrium phase-space theory to treat non-equilibrium systems. Their 'linear response' theory is valid for non-equilibrium systems not too far from equilibrium. Green and Kubo discovered that the transport coefficients (such as Newton's viscosity and Fourier's heat conductivity) are given by the rates of decay of appropriate fluctuations [1]. Pressure tensor fluctuations give the bulk and shear viscosities. For example, the shear viscosity η depends upon the ensemble-averaged decay of the xy components of the pressure tensor:

$$\eta kT/V = \int_0^\infty \langle P_{xy}(0)P_{xy}(t) \rangle \, dt.$$

Heat flux vector fluctuations give the conductivity. It is essential that these decays be averaged and it is again paradoxical that irreversible behaviour can be consistent with underlying reversible dynamics.

When these Green–Kubo expressions were first tried out, using a pair potential expected to provide a rough description of inert-gas liquids, and compared with experimental results for those liquids, the agreement was quite disappointing [8, 26]. Direct non-equilibrium simulations were developed as an alternative. Those helped to uncover the mistakes in the analysis of the equilibrium simulation work, and showed that Green and Kubo's theory was quite correct.

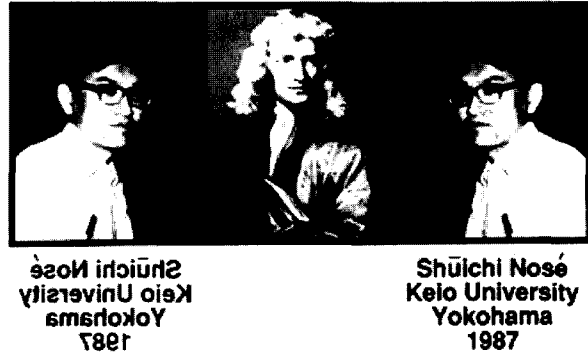Two main types of non-equilibrium simulation were developed: externally driven flows, with boundary

Figure 5. A system obeying classical Newtonian mechanics is sandwiched between two Nosé–Hoover reservoirs. When the reservoirs have differing mean velocities or differing temperatures a non-equilibrium steady state, with a fractal phase-space distribution, can result, despite the formal time reversibility of the equations of motion in both the central Newtonian region and the Nosé–Hoover reservoirs. Shear viscosity and heat conductivity may be 'measured' by using simulations with this geometry.

regions, and homogeneous flows [1, 26–29], driven by internal fields. Externally driven flows of momentum or heat could be driven through a central Newtonian region sandwiched between two boundary regions, with the boundary regions' velocities and temperatures constrained to constant values. A caricature simulation is shown in figure 5. Special time-reversible 'thermostat forces', described in the next section, had to be developed to impose the constraints in the external boundary regions.

Homogeneous internal driving fields for non-equilibrium momentum and heat flows also have been derived. The fields used are fully consistent with Green–Kubo theory [29]. Just as is the case for external driving, special thermostat forces are required to extract the heat generated internally by homogeneous irreversible flows. The non-equilibrium simulations not only showed good agreement with laboratory experiments. They also showed that only a few particles need be used to obtain good estimates for the transport coefficients.

To illustrate the simplest possible small-system flow [1, 30, 31], consider again two hard discs, but this time with the periodic boundaries appropriate to a triangular lattice structure. In the absence of any driving field the dynamics are simple, with the discs moving along straightline trajectories between collisions. Beginning with a non-overlapping, but otherwise arbitrary, initial condition the discs may be advanced for a small time interval dt:
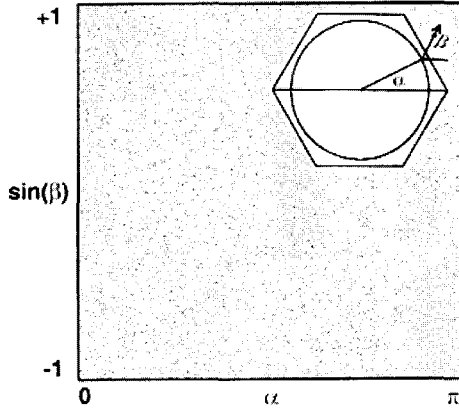
$$r(t + dt) = r(t) + v(t)\,dt; \qquad v(t + dt) = v(t).$$

Figure 6. The field-free motion of two hard discs leads to a collision sequence that fills the $(\alpha, \sin\beta)$ plane uniformly. The two angles define the location and relative velocity of successive collisions, as shown in the inset. The dynamics have been simplified by choosing a coordinate system fixed on one of the particles, as is described in section 7.

These dynamics conserve energy exactly, with the kinetic energy a constant of the motion. Whenever the two discs interpenetrate at the end of such a timestep, they are replaced at their previous coordinates with their relative velocities reversed. A sequence of just over 150 000 equilibrium collisions obtained in this way, with no accelerating field, is shown in figure 6. The simulation is quite consistent with the theoretical result that all accessible phase-space states are eventually visited by this simple two-disc system.

Now imagine a more complicated situation in which an external field F drives one of the discs to the right and the other to the left. A corresponding simulation may be carried out readily, advancing the coordinates and velocities of each disc with simple leapfrog dynamics:

$$r(t + dt) = r(t) + v\left(t + \frac{dt}{2}\right) dt;$$

$$v_x\left(t + \frac{dt}{2}\right) = v_x\left(t - \frac{dt}{2}\right) \pm \frac{F}{m} dt;$$

$$v_y\left(t + \frac{dt}{2}\right) = v_y\left(t - \frac{dt}{2}\right).$$

The simulation can be simplified by using coordinates fixed on one of the discs. Then the other one moves as before in response to the field, but with velocity $2v$ rather than v and with the reduced mass $m/2$. Such a simulation, though stable, is far from well behaved, with large fluctuations of the discs' kinetic energy superimposed on a positive drift.

To characterize a non-equilibrium stationary state it is necessary to prevent this long-term energy drift so

as to maintain the system in a non-equilibrium steady, as opposed to transient, state. This can be done by constraining the kinetic energy, $mv^2/2 \equiv mv_0^2/2$, by a velocity-rescaling procedure discussed in more detail in the following section. The kinetic energy is a useful non-equilibrium state variable, just as is temperature at equilibrium.

The many more-general equilibrium thermostat approaches [32–35] have a common defect when applied to non-equilibrium systems. They specify more than the minimum necessary about the form of f, thereby adding artificial dissipation to the dynamics. Specifying more than the instantaneous or time-averaged second moment, v^2 or $\langle v^2 \rangle$, unnecessarily breaks the microscopic-to-macroscopic connection that follows from the simple feedback form of the Nosé–Hoover thermostat.

The constrained velocity rescaling dynamics reduce to a simple three-step algorithm:

$$\tilde{v}_x\left(t + \frac{dt}{2}\right) = v_x(t) + \frac{F\,dt}{2m}; \qquad \tilde{v}_y\left(t + \frac{dt}{2}\right) = v_y(t);$$

$$r(t + dt) = r(t) + \tilde{v}\left(t + \frac{dt}{2}\right) dt;$$

$$v(t + dt) = \tilde{v}\left(t + \frac{dt}{2}\right)\left[\frac{v_0^2}{\tilde{v}\left(t + \frac{dt}{2}\right)^2}\right]^{1/2}.$$

The last step guarantees that the kinetic energy maintains its original value. Collision sequences generated in this stationary non-equilibrium situation are qualitatively different from the smooth equilibrium distribution of figure 6. Figure 7 shows a two-disc example. This two-disc distribution is in fact fractal, with fractional dimensionality and singular everywhere. Fractal distributions are discussed in more detail in sections 9 and 10 [1, 3–5, 30, 31, 36].

So far, there is no useful theoretical treatment of non-equilibrium systems that goes beyond Green and Kubo's linear-response theory. That approach uses the smooth equilibrium distribution function $f(q, p, t)$ as a basis for non-equilibrium averages. The singular character of non-equilibrium distributions makes them particularly hard to treat from a theoretical standpoint. The lack of a convergent perturbation theory about equilibrium suggests that non-equilibrium systems have to be treated on a case-by-case basis rather than on the basis of general deductive rules.

Computer simulations of non-equilibrium systems are not so limited. Appropriate driving and thermostating forces make it possible to simulate a wide variety of non-equilibrium systems. Such simulations have a 50 year
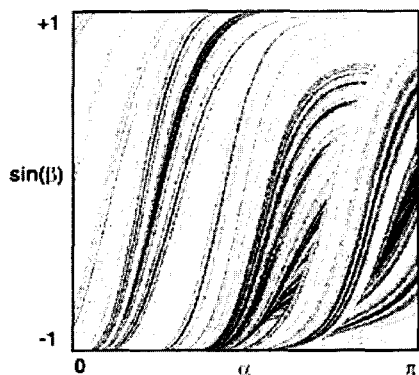
Figure 7. By adding (i) an accelerating field driving one disc to the right and the other to the left and (ii) an isokinetic (velocity rescaling) thermostat fixing the kinetic energy, the two-disc system of figure 6 becomes dissipative, with successive collisions defining a fractional dimensional strange attractor. The corresponding non-equilibrium phase-space volume is reduced in dimensionality, rather than in size. The information dimension is 1.8 and the correlation dimension is 1.6 for the field strength used here.

history. Just after World War II Fermi analysed the dynamics of non-linear chains at Los Alamos [37] in an effort to measure equilibration rates. He was surprised to find no tendency towards equilibration. A few years later, at Livermore, Alder and Wainwright [38] found that hard discs and hard spheres equilibrate rapidly. Vineyard [39], at Brookhaven, used continuous potentials to model the equilibration of highly energetic copper atoms in the solid phase, carrying out innovative radiation damage studies. Shockwave studies at Livermore and Los Alamos [40, 41] also indicated rapid convergence to a non-equilibrium steady state with realistic continuous potentials. The shockwave problem is the prototypical problem for studying nonlinear transport: the spatial scale of the phenomenon is small and the nonlinear effects are large, with the ratio of the longitudinal and transverse temperatures as large as 2 [41]. Thorough analyses of these results from computer simulation are still beyond the reach of presentday theoretical treatments, but the combination of computer simulation and theoretical analysis promises to clarify far-from-equilibrium behaviour.

8. Time-reversible thermostats

It is essential, in any steady-state non-equilibrium work, to use thermostats to extract the extra heat generated. Shortly after 1900 Langevin developed stochastic forces that would drive an initial velocity distribution towards the equilibrium Maxwell–Boltzmann distribution. In the presence of non-equilibrium driving forces the Langevin stochastic forces lack the feedback necess-

ary to obtain a definite specified temperature. This limits the usefulness of the Langevin approach. Typically, numerical implementations of 'stochastic' forces lack the reproducibility so necessary for collaborative work. Straightforward 'velocity scaling', as illustrated in figure 7, multiplying each velocity in a thermostated region by a constant to keep the overall kinetic energy fixed, is perhaps the simplest reproducible 'thermostat'. The specified temperature is reproduced exactly, in this way.

In 1984 Nosé developed a more general, but still completely deterministic and reproducible, method based on Hamiltonian mechanics [42]. His approach made it possible to follow changes in the comoving phase-space density f as a function of time. The previous velocity-scaling work of Woodcock and Ashurst turned out to be a special case of Nosé's thermostat. That special case has been termed the 'Gaussian thermostat' because it can be generated using Gauss' 'principle of least constraint' [43]. Further and slightly more complicated generalizations, sufficient to thermostat an equilibrium harmonic oscillator, were developed later, by several groups of workers [32–35]. These later thermostats, being based on the goal of reproducing the Maxwell–Boltzmann distribution at equilibrium, are not so suitable for simulations far from equilibrium as are the Gaussian and Nosé–Hoover thermostats.

Like Langevin's stochastic thermostat, Nosé's is directed towards enforcing a prescribed kinetic energy for each Cartesian degree of freedom. Though Nosé's thermostat is perfectly consistent with the equilibrium velocity distribution it does not attempt to impose this distribution far from equilibrium. Particles thermostated with the simplest 'Nosé–Hoover' form of Nosé's thermostat are acted on with a non-Hamiltonian thermostat force that incorporates an arbitrary response time τ:

$$\dot{q} = \frac{p}{m}; \qquad \dot{p} = F(q) - \zeta p;$$

$$K_{eq}(T)\tau^2 \dot{\zeta} = K - K_{eq}(T).$$

These Nosé–Hoover motion equations are, like Hamilton's equations, time reversible. However, they exhibit a new feature: the comoving phase-space density $f(q, p, \zeta, t)$ changes with time, as heat is exchanged through the thermostat friction coefficient ζ. Evidently the rate at which heat is extracted by the Nosé–Hoover thermostat forces is

$$\dot{E}_Q = T\dot{S} = \sum \zeta p^2/m,$$

where the sum includes all thermostated degrees of freedom. Because the time-averaged time derivative of ζ^2 must vanish in any stationary state,

$$K_{eq}(T)\tau^2\langle\zeta\dot\zeta\rangle = 0 = \langle\zeta K\rangle - \langle\zeta\rangle K_{eq}(T),$$

$$\longrightarrow \langle\zeta K\rangle = \langle\zeta\rangle K_{eq}(T),$$

and the Nosé–Hoover entropy production $\dot{S}_{NH}$ can be simplified:

$$\langle\dot{S}_{NH}/k\rangle \equiv \langle\dot{E}_Q/kT\rangle = \left\langle\sum \zeta p^2/mkT\right\rangle = \left\langle\sum\zeta\right\rangle.$$

This simple link between the microscopic thermostat variable ζ and the macroscopic entropy production $\dot{S}$ is a special advantage of the Nosé–Hoover thermostat. Despite the changing phase-space probability density, any coordinate sequence satisfying the Nosé–Hoover equations can have its time order reversed and is still a solution of the equations. In the reversal process both p and ζ change sign.

In the absence of external forces driving the system away from equilibrium, these 'Nosé–Hoover' equations of motion incorporating the feedback forces $\{-\zeta p\}$ are perfectly consistent with Gibbs' canonical distribution. At equilibrium f also has a Gaussian dependence on the friction coefficient ζ:

$$f \propto e^{-H/kT}e^{-(\#/2)(\tau\zeta)^2},$$

where $\#$ is the number of thermostated degrees of freedom. Although Nosé's goal was dynamics which could reproduce Gibbs' equilibrium phase-space distributions, exactly the same approach also may be applied away from equilibrium too. This approach turns out to have fundamental importance for the interpretation of the fractal distributions that arise away from equilibrium. The changing phase-space density, due to the presence of the friction coefficient ζ, makes fractal solutions possible.

9. Fractal phase-space distributions and Lyapunov instability

When the Nosé–Hoover equations of motion are applied in a non-equilibrium situation (the simplest case is the two-reservoir sandwich system shown in figure 5), we have seen that the phase-space flow is no longer phase-volume preserving. In fact, in a stationary non-equilibrium situation, the comoving phase volume approaches zero, as we detail next.

The probability density change following a Nosé–Hoover flow in the 'extended' $\{qp\zeta\}$ phase space is still given by a phase-space continuity equation, but with $\partial\dot{p}/\partial p$ equal to $-\zeta$ rather than 0 and with $\partial\dot\zeta/\partial\zeta = 0$:

$$\dot{f} = \frac{\partial f}{\partial t} + \sum \dot{q}\frac{\partial f}{\partial q} + \sum \dot{p}\frac{\partial f}{\partial p} + \sum \dot\zeta\frac{\partial f}{\partial\zeta}$$

$$\equiv -f\sum\left[\frac{\partial\dot{q}}{\partial q} + \frac{\partial\dot{p}}{\partial p} + \frac{\partial\dot\zeta}{\partial\zeta}\right]$$

$$= -f\sum [0 - \zeta + 0]$$

$$= f\sum\zeta \neq 0.$$

If the boundary conditions driving the system away from equilibrium are stationary then the time-averaged derivative $\langle\dot{f}/f\rangle = \langle\sum\zeta\rangle$ must be either positive or negative. The positive sign corresponds to a singular divergent probability density, like that shown in figure 7. Evidently the negative sign would correspond to a vanishing probability density, impossible in any finite region of phase space. (The excluded alternative, $\langle\dot{f}/f\rangle = 0$, corresponds to thermal equilibrium.)

Because f must change, away from equilibrium, with the sign of $\langle\dot{f}/f\rangle$ given by the sign of $\langle\zeta\rangle$, a steady state can be characterized by only two values of $\langle f\rangle$, zero and infinity. Because zero probability density is impossible in any finite phase volume, the distribution induced by heat transfer must instead converge, infinitely densely, $\langle f\rangle \to \infty$, and singularly, onto those attracting phase-space states describing a macroscopic stationary non-equilibrium state. Thus any non-equilibrium stationary state occupies a vanishingly small region of the equilibrium phase space. In this small region at least one of the non-equilibrium fluxes (mass, momentum, energy) has a non-vanishing average. The collapse of the probability density onto a non-equilibrium attractor is driven by the boundary (thermostat) interactions, which transfer heat from the non-equilibrium system to its surroundings. The collapse rate, which turns out to be a direct instantaneous measure of the entropy production, is best described through the instantaneous Lyapunov spectrum λ or its time average $\langle\lambda\rangle$. For a step-by-step illustration of the collapse process for the Galton board fractal distribution, shown in figure 7, see [1], figure 11.4.

The deformation of the phase volume $\otimes$ defines the spectrum of local and global (or time-averaged) 'Lyapunov exponents' λ and $\langle\lambda\rangle$, respectively. These are instantaneous logarithmic strain rates of the local rates of stretching or shrinking of the principal axes of a comoving hyperellipsoid in phase space, and their long-term averages. The total number of Lyapunov exponents corresponds to the number of distinct dimensions in the phase space where the motion is described, with the sum of all the exponents giving the rate at which the comoving phase volume changes with time:

$$\sum \lambda = \frac{\dot{\otimes}}{\otimes} \longrightarrow \sum \langle \lambda \rangle = \left\langle \frac{\dot{\otimes}}{\otimes} \right\rangle.$$

The Lyapunov exponents, depending as they do on perturbations of model equations of motion, are not directly available from laboratory experiments. There are ways to extract these exponents from time series of experimental data (assuming that the boundary conditions on the experiment are stationary), but the lack of precision and the lack of stationary boundary conditions characterizing any real experiment renders this approach impotent.

During the past 15 years considerable effort has established the nature of these non-equilibrium distributions: most typically they are ergodic (visiting all the accessible phase space from any initial condition). The distributions are also 'fractal' objects (with the integrated density about a point varying as a fractional power of the distance from that point) [1, 3, 4, 30, 31, 36].

Let us consider the two-particle Galton board example of section 7 [1, 4, 30, 31, 44]. If the fractal phase-space cross-section shown in figure 7 is decomposed into δ^{-2} cells with dimensions $\pi\delta \times 2\delta$, this grid of cells allows the attractor to be characterized by the size-dependent cell probabilities $\{p_c(\delta)\}$. For an ordinary probability density, such as that shown in figure 6, the cell probabilities would all vary as δ^2 for small δ and the 'information' (the negative of the entropy in units of Boltzmann's constant) would be computed as the small-δ limit of the sum $\sum p_c \ln(p_c/\delta^2)$. For the fractal distribution shown in figure 7 this sum over infinitesimal cells,

$$-\frac{S_{\text{info}}}{k} \equiv \langle \ln f \rangle = \left\langle \ln\left(\frac{p_c}{\delta^2}\right) \right\rangle = \sum p_c \ln\left(\frac{p_c}{\delta^2}\right),$$

does not converge, and instead varies as $-0.2 \ln \delta$, so that the information entropy diverges, to minus infinity, for zero cell size. Accordingly, the 'information dimension' of this fractal attractor is said to be $D_{\text{info}} = 2 - 0.2 = 1.8$ rather than the dimensionality of the sample space 2.0.

In most cases this information dimension is also equal to the Kaplan–Yorke dimension D_{KY} [36], the (linearly interpolated) number of exponents at which the sum of D_{KY} long-term averaged Lyapunov exponents changes sign, from positive to negative:

$$\sum_{k=1}^{D_{\text{KY}}} \langle \lambda_k \rangle = \left\langle \frac{\dot{\otimes}_{D_{\text{KY}}}}{\otimes_{D_{\text{KY}}}} \right\rangle \equiv 0.$$

Any phase-space object with a dimensionality less than D_{KY} grows without bound, while any phase-space object with a higher dimensionality vanishes after long times.

For an ordinary probability density in two dimensions, the probability of finding two points sampled

according to the density within a small distance δ of one another is proportional to δ^2. For the fractal distribution shown in figure 7 a double logarithmic plot of probability as a function of separation indicates that the probability varies as the 1.6 power of the separation δ. Accordingly, the attractor is said to have a 'correlation dimension' D_2 of 1.6. Additional dimensions $D_3, D_4, \ldots$ can be defined by considering triples, quadruples, ... of points. The fractal nature of a fractal distribution may be characterized, in part, by these fractal dimensions [36]. For small deviations from equilibrium the fractal dimensions vary quadratically with the magnitude of the gradient or external force driving the system away from equilibrium.

We have seen that the rate at which the comoving phase volume contracts onto the fractal attractor is closely related to the external entropy production whenever Nosé–Hoover thermostats are used. The non-equilibrium version of Liouville's theorem in this case,

$$\frac{\dot{f}}{f} = -\frac{\dot{\otimes}}{\otimes} \equiv \sum \zeta_{\text{NH}},$$

establishes the connection. It has been argued that the generality of this relation in its application to large systems still needs to be established [35]. However, simulations based on Nosé–Hoover dynamics establish very clearly, despite the formal time-reversibility of the underlying microscopic equations of motion, that there is a paradoxical irreversible flow from a fractal repellor to a mirror-image strange attractor [45]. Though both these phase-space objects are unstable, the repellor is invariably even less stable than is the attractor, so that only the attractor is ever observed.

Thus the microscopic phase-space continuity equation $\dot{f}/f = \sum \zeta = \dot{S}/k$ makes contact with nonlinear dynamics, as well as with the entropy production of macroscopic irreversible thermodynamics. It is possible to understand the difference in time symmetry between the microscopic and macroscopic view in detail by considering the Lyapunov spectrum description of the phase-space dynamics. The Lyapunov spectrum is symmetric at equilibrium, with the exponents occuring in pairs $\{\pm\lambda\}$. This symmetry is broken away from equilibrium.

10. Irreversibility from reversible dynamics

The time symmetry of Hamilton's (equilibrium) equations of motion guarantees that every phase-space direction corresponding to expansion (with a positive Lyapunov exponent $+\lambda$) is paired with a corresponding orthogonal phase-space direction (with reversed momenta) for which the Lyapunov exponent is negative, $-\lambda$. In accordance with the second law of thermody-

namics, this Lyapunov exponent symmetry is lost away from equilibrium. Instead the dynamics, while formally reversible, become irreversible in fact, and in an interesting way. The phase-space motion forward in time is more stable numerically than is the reversed motion. For this reason the reversed motion is not observable. The summed-up spectrum of Lyapunov exponents, zero at equilibrium, becomes negative away from equilibrium (indicating collapse to a fractional-dimensional distribution). The reversed trajectory, which would have a positive Lyapunov sum, is simply unobservable. In some simple homogeneous cases the shift of each separate pair of Lyapunov exponents towards more negative values is uniform, with the same shift for every pair of exponents. This shift has been explained in quantitative detail by Dettmann and Morriss [46].

For a good illustration of this exponent shift consider the many-body analogue of the field-driven problem of section 7 [47, 48]. If the kinetic energy of the system is constrained to a constant value by using a Nosé–Hoover thermostat, the non-equilibrium spectrum looks very much like the equilibrium one, with each exponent shifted towards more negative values. The total summed-up spectrum is identically equal to minus the overall rate of dissipation, $\dot{S}/k$. This equality provides a chain of identities linking together the microscopic Lyapunov exponents, the changing phase volume, the diverging phase-space probability density and the macroscopic entropy production:

$$-\sum \lambda \equiv -\frac{\dot{\otimes}}{\otimes} \equiv +\frac{\dot{f}}{f} \equiv +\sum \zeta \equiv \frac{\dot{S}}{k}.$$

Figure 8 illustrates the shift of a 32-body Lyapunov spectrum from symmetric to more negative values in response to dissipation. Figure 9 illustrates a structural phase transition in a much larger system of 25,600 particles. Here the larger of the two fields for which results are shown is enough to separate the two types of particle from one another.

It seems likely that generally the connection between the Lyapunov exponents of a properly thermostated non-equilibrium flow, the fractal character of the phase-space distribution function, and the macroscopic entropy production is valid in an appropriate large-system limit, with the most straightforward approach being based on the Nosé–Hoover motion equations. It is to be expected (an article of faith rather than a theorem) that other types of thermostat lead to essentially similar results [49] even though poor choices, which unduly restrict the distribution at the system boundary, can destroy the exact correlation by adding additional spurious dissipation within the boundaries themselves. The entropy production, or the Lyapunov exponents
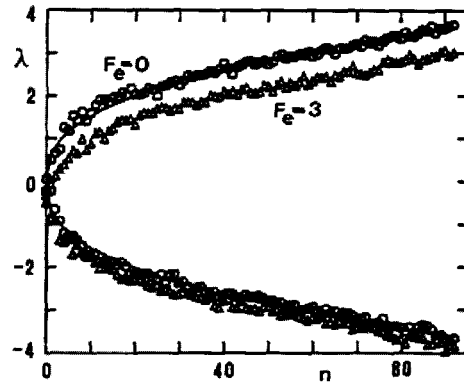

Figure 8. Lyapunov spectrum of a 32 particle system with 'realistic Lennard-Jones' forces. Half the particles are driven to the right and half to the left by an external field. Both the equilibrium (zero field) and non-equilibrium spectra are shown in this figure. This pioneering simulation was carried out in 1987 [48].

Figure 9. Snapshots of a many-body system of $N = 25600$ particles, half of which are driven to the right and half to the left by an external field, as in figure 7. At the higher field strength the two species are separated by the field. The kinetic temperature is thermostated by continuous velocity rescaling. The symmetric spectrum, obtained with the field off, is shifted towards more negative values with the field turned on, indicating a loss of phase-space dimensionality away from equilibrium. In the upper example the dimensionality loss is about 170.

themselves, give some novel information about the phase-space distribution. It converges onto a strange attractor with a dimensionality, not just a volume, smaller than the equilibrium one. Thus the rarity of non-equilibrium states is qualitative in nature, not just quantitative.

The change of phase volume is fundamental for a mechanical understanding of irreversibility. The irreversibility is the result of instability, with the forward direction of time less unstable than the backward one. The future is more nearly predictable than is the past. This is yet another way to express the second law of thermodynamics. The difficulty of retrodiction, relative to prediction, can be quantified through the Lyapunov spectrum. Any attempt to reverse a non-equilibrium trajectory, lacking perfect knowledge of it, fails due to the very rapid growth of non-equilibrium fluctuations.

11. Present understanding of fluid mechanics

Fifty years of computer simulation have given us a good understanding of fluids, not only from Newton's and Hamilton's atomistic point of view, Gibbs' and Boltzmann's ensemble point of view and Euler's and Lagrange's continuum point of view, but also from an intermediate smooth particle view. SPAM introduced a kind of averaging additional to and complementary to time averaging, space averaging and ensemble averaging. The old puzzle of irreversible behaviour from strictly time-reversible motion equations has been solved too. It is the presence of chaos that makes the observable motion-equation solutions forward in time,

$$q_1, q_2, \ldots, q_{n-1}, q_n,$$

less unstable than the corresponding unobservable time-reversed trajectories,

$$q_n, q_{n-1}, \ldots, q_2, q_1.$$

The classic particle, ensemble and continuum formulations of fluids have all been enriched by contributions from chaos and fractal geometry, leading to a new understanding of the irreversibility underlying the second law of thermodynamics.

References

[1] HOOVER, WM. G., 1991, *Computational Statistical Mechanics* (Amsterdam: Elsevier).
[2] VESELY, F., 1994, *Computational Physics: An Introduction* (New York: Plenum Press).
[3] HOOVER, WM. G., 1998, *J. chem. Phys.*, **109**, 4164.
[4] HOOVER, WM. G., 1999, *Time Reversibility, Computer Simulation and Chaos* (Singapore: World Scientific).
[5] HOOVER, WM. G., 1998, *Physica* D, **112**, 225; see also related papers in this volume, which is the Proceedings of the Workshop on Time-Reversal Symmetry in Dynamic Systems held at Warwick University in December 1996.
[6] HOLIAN, B. L., HOOVER, W. G., and POSCH, H. A., 1987, *Phys. Rev. Lett.*, **59**, 10.
[7] RUELLE, D., 1999, *J. statist. Phys.*, **95**, 393.
[8] LEVESQUE, D., VERLET, L., and KÜRKIJARVI, J., 1973, *Phys. Rev.* A, **7**, 1690.
[9] LEVESQUE, D., and VERLET, L., 1993, *J. statist. Phys.*, **72**, 519.
[10] ALDER, B. J., HOOVER, W. G., and WAINWRIGHT, T. E., 1963, *Phys. Rev. Lett.*, **11**, 241.
[11] FORD, J., 1989, *The New Physics*, edited by P. Davies (Cambridge University Press) p. 348.
[12] RAMSHAW, J. D., 2002, *Europhys. Lett.*, **59**, 319.
[13] KUM, O., and HOOVER, W. G., 1994, *J. statist. Phys.*, **76**, 1075.
[14] MONAGHAN, J., 1992, *Ann. Rev. Astron. Astrophys.*, **30**, 543.
[15] LUCY, L., 1977, *Astron. J.*, **82**, 1013.
[16] KUM, O., HOOVER, WM. G., and POSCH, H. A., 1995, *Phys. Rev.* E, **52**, 4899.
[17] HOOVER, W. G., and KUM, O., 1995, *Molec. Phys.*, **86**, 685.
[18] HOOVER, WM. G., POSCH, H. A., CASTILLO, V. M., and HOOVER, C. G., 2000, *J. statist. Phys.*, **100**, 313.
[19] HOOVER, WM. G., and HOOVER, C. G., 2001, *Comput. Sci. Eng.*, **3**, 78.
[20] HOOVER, W. G., HOLIAN, B. L., and POSCH, H. A., 1993, *Phys. Rev.* E, **48**, 3196.
[21] WHEELER, L. P., 1951, *Josiah Willard Gibbs: The History of a Great Mind* (New Haven, CT: Yale University Press).
[22] CERCIGNANI, C., 1998, *Ludwig Boltzmann: The Man Who Trusted Atoms* (Oxford University Press).
[23] HOOVER, W. G., and REE, F. H., 1968, *J. chem. Phys.*, **49**, 3609.
[24] GREEN, M. S., 1951, *J. chem. Phys.*, **19**, 1036.
[25] KUBO, R., 1957, *J. Phys. Soc. Jap.*, **12**, 570.
[26] ASHURST, W. T., and HOOVER, W. G., 1975, *Phys. Rev.* A, **11**, 658.
[27] HOOVER, W. G., 1983, *Physica* A, **118**, 111.
[28] HOOVER, W. G., 1984, *Phys. Today*, January, 44.
[29] EVANS, D. J., and MORRISS, G. P., 1990, *Statistical Mechanics of Nonequilibrium Liquids* (New York: Academic Press).
[30] MORAN, B., HOOVER, W. G., and BESTIALE, S., 1987, *J. statist. Phys.*, **48**, 709.
[31] CHERNOV, N. I., EYINK, G. L., LEBOWITZ, J. L., and SINAI, Y. G., 1993, *Phys. Rev. Lett.*, **70**, 2209.
[32] KUSNEZOV, D., BULGAC, A., and BAUER, W., 1990, *Ann. Phys.*, **204**, 155; 1992, *Ann. Phys.*, **214**, 180.
[33] HOOVER, WM. G., and HOLIAN, B. L., 1996, *Phys. Lett.* A, **211**, 253.

[34] MARTYNA, G. J., KLEIN, M. L., and TUCKERMAN, M., 1992, *J. chem. Phys.*, **97**, 2635.

[35] RATEITSCHAK, K., and KLAGES, R., 2002, *Phys. Rev. E*, **65**, 036209.

[36] FARMER, J. D., OTT, E., and YORKE, J. A., 1983, *Physica D*, **7**, 153.

[37] TUCK, J. L., and MENZEL, M. T., 1972, *Adv. Math.*, **9**, 399.

[38] ALDER, B. J., and WAINWRIGHT, T. E., 1959, *Sci. Amer.*, **201**, 113.

[39] GIBSON, J. B., GOLAND, A. N., MILGRAM, M., and VINEYARD, G. H., 1960, *Phys. Rev.*, **120**, 1229.

[40] HOLIAN, B. L., HOOVER, W. G., MORAN, B., and STRAUB, G. K., 1980, *Phys. Rev. A*, **22**, 2798.

[41] KUM, O., HOOVER, WM. G., and HOOVER, C. G., 1997, *Phys. Rev. E*, **56**, 462.

[42] NOSÉ, S., 1984, *J. chem. Phys.*, **81**, 511.

[43] HOOVER, W. G., 1995, *Phys. Lett.* A, **204**, 133.

[44] DELLAGO, CH., 1995, Ph.D. thesis, University of Vienna.

[45] HOOVER, WM. G., POSCH, H. A., AOKI, K., and KUSNEZOV, D., 2002, *Europhys. Lett.*, in press.

[46] DETTMANN, C. P., and MORRISS, G. P., 1996, *Phys. Rev. E*, **53**, R5545.

[47] POSCH, H. A., and HOOVER, W. G., 1989, *Phys. Rev. A*, **39**, 2175.

[48] POSCH, H. A., and HOOVER, W. G., 1987, *Abstracts of the Europhysics Liquid State Conference on Liquids of Small Molecules*, Santa Trada, Italy, 21–25 September (European Physical Society) p. 17.

[49] EVANS, D. J., and HOLIAN, B. L., 1985, *J. chem. Phys.*, **83**, 4069.